Trellis-Coded Modulation-Enabled Probabilistic Shaping With Simplified Viterbi Decoder for Bandwidth-Limited IMDD Systems

Han Cui, Zhongliang Sun, Xiaoqian Huang, Du Tang, Fei Xie, and Yaojun Qiao

***Abstract*—In this article, trellis-coded modulation-enabled probabilistic shaping (TEPS) scheme with a simplified Viterbi decoder is proposed. Trellis-coded modulation (TCM) is embedded in the probabilistic shaping (PS) technique to improve the performance of PS signals in bandwidth-limited intensity modulation and direct detection (IMDD) systems. Further, to reduce the calculation complexity of TCM decoding, the constellation partition decision-assisted (CPDA)-Viterbi decoder is proposed which decides the received signal before decoding to reduce the branches. To verify the performance of the proposed scheme, a 32-GBaud TEPS-four-level pulse-amplitude modulation (PAM4) experimental system with 10G-class O-band directly-modulated laser (DML) is built over a 20-km standard single-mode fiber (SSMF) transmission link. The experimental results show that TEPS-PAM4 achieved up to 1.80-dB higher receiver sensitivity than PS-PAM4 at 7% forward error correction (FEC) limit with the same net rate. Moreover, with the multiplications reduced by up to 45.7% compared with the Viterbi decoder, TEPS-PAM4 with CPDA-Viterbi decoder has up to 1.50-dB higher receiver sensitivity limit than PS-PAM4 at 7% FEC.**

***Index Terms*—Probabilistic shaping, trellis-coded modulation, bandwidth-limited, IMDD system, Viterbi decoder.**

I. Introduction

THE rapid development of bandwidth-hungry applications such as cloud computing, multimedia services, social networking and high-definition (HD) video drive the capacities of optical fiber communication systems to higher and higher [1], [2], [3]. In short-reach transmission scenarios, coherent transmission systems are widely discussed because of their high capacity availability, which can meet the increasing demand for capacity growth [4], [5]. However, due to their high cost and power consumption, they are currently not applicable in cost-sensitive scenarios [6]. In contrast, intensity modulation and direct detection (IMDD) is generally adopted for short-reach optical transmission due to its low cost, low power consumption and low complexity [7], [8]. In addition, the directly-modulated laser (DML) is preferable to further reduce cost per bit thanks to its low cost, small footprint, relatively low drive voltage, and high optical output power [9], [10], [11]. The bandwidth of a low-cost DML is usually narrow, and other cost-effective opto-electronics can also result in limited system bandwidth, making it challenging to further increase the information rate [12], [13]. In the IMDD system, different modulation and coding schemes have different characteristics and advantages [14], [15], [16]. For example, high-order modulation formats are more spectrally efficient than low-order modulation formats. However, their noise immunity is not as good as low-order modulation schemes. In addition, coding schemes can improve bandwidth utilization by compressing the signal spectrum, such as the non-linear differential coding scheme [17], [18]. However, severe inter-symbol interference (ISI) is introduced. By adopting suitable modulation and coding schemes, higher data transmission rates and improved signal quality can be achieved under limited bandwidth conditions. Therefore, for the bandwidth limitation of the IMDD optical fiber communication system, it is very important to study the appropriate modulation and coding scheme to overcome the bandwidth limitation and improve the system performance.

Probabilistic shaping (PS) techniques have been incorporated into optical transmission systems in order to reduce the gap between capacity and the Shannon limit [19]. In additive white Gaussian noise (AWGN) channels, the PS can provide a maximum theoretical shaping gain of 1.53 dB [20]. The probabilistic amplitude shaping (PAS) architecture is proposed in which the distribution matcher (DM) and forward error correction (FEC) code are combined [21]. The DM is responsible for generating amplitudes with a probability distribution, while the uniformly distributed parity bits of FEC coding are used as sign bits which ensure that they will not affect the probability distribution of the signal. In recent years, the application of PS technology in IMDD systems has become a hot research topic, one of the reasons being that PS signals allow for more flexible adjustment of system rates. The proposed flexible rate adjustment scheme can be divided into multi-carrier schemes [22] and single-carrier schemes. In the single-carrier scheme, the rate can be adjusted by PS technology which could jointly adjust entropy and FEC code rate, and a net transmission rate from 86.7 Gbit/s to 36.65 Gbit/s is achieved [23]. Another advantage of PS technology is that it can improve receiver sensitivity. There are results that show that the PS-PAM4 signal is significantly better than the

Manuscript received 17 August 2023; revised 5 September 2023; accepted 7 September 2023. Date of publication 11 September 2023; date of current version 22 September 2023. This work was supported in part by the National Natural Science Foundation of China under Grant 62271080, and in part by Fund of State Key Laboratory of IPOC (BUPT) under Grant IPOC2022ZT06. *(Corresponding author: Yaojun Qiao.)*

The authors are with the State Key Laboratory of Information Photonics and Optical Communications, School of Information and Communication Engineering, Beijing University of Posts and Telecommunications, Beijing 100876, China (e-mail: qiao@bupt.edu.cn).

Digital Object Identifier 10.1109/JPHOT.2023.3314028

ordinary PAM4 signal in improving signal transmission rate and the tolerance to the bandwidth limitation [24]. The results also confirm that if the system bandwidth is limited, PS can provide a considerable shaping gain, which may result in a large peak-to-average power ratio (PAPR) [25], [26]. However, for limited-budget IMDD systems with strict bandwidth limitations which lead to more severe channel degradation, there is still room for improvement in PS signal performance.

Furthermore, trellis-coded modulation (TCM) is a powerful modulation scheme, which can achieve significant coding gain and robust error correction with relatively simple coding by combining coding and modulation [27], [28], [29]. TCM was first proposed by G. Ungerboeck in 1982 [30], and it has been investigated in optical transmission systems due to excellent error correction [31], [32], [33], [34], [35]. Compared to PAM4, 2D-TCM-PAM4 can provide about 2.8 dB gain over 40-km standard single-mode fiber (SSMF) transmission [31]. The 2D-TCM-PAM8 was used in an experimental demonstration of a 50-Gb/s PON system based on 10G-class O-band DML. Compared to PAM6, the receiver sensitivity of 2D-TCM-PAM8 is improved by 1.1 dB over 20-km transmission [32]. Additionally, the Viterbi decoder is required at the receiver. However, the complexity of the Viterbi decoding algorithm is high. In addition, the integration of PS and TCM technologies presents an attractive potential for improving spectral efficiency and bit error performance. It is worth noting that there has been pioneering related research in both voice-band modems and digital subscriber line (DSL) electrical communication systems [36], [37]. In voice-band modems electrical communication systems, the scheme of combining PS and TCM is proposed, in which PS is implemented by a Shell mapper [36]. In DSL electrical communication systems, PS technology is combined with low density parity check-coded modulation (LCM), where LCM is based on set partitioning like TCM [37]. The importance of the above two schemes cannot be overstated as they offer feasible approaches for the integration of PS and TCM. However, the above schemes are all applied to pure electrical transmission systems. The research and implementation of the integration of PS with TCM in IMDD optical fiber transmission systems is still an unexplored field.

In order to improve the tolerance of PS-PAM signal to bandwidth limitation in IMDD optical fiber transmission systems, TCM enabled PS (TEPS) scheme is proposed in this article. Further, the constellation partition decision-assisted (CPDA)-Viterbi decoder is proposed to reduce the calculation complexity of decoding. We demonstrated a 32-GBaud TEPS-PAM4 IMDD optical system with 10G-class O-band DML over 20-km SSMF transmission. The main contributions of this article are:

- We propose the TEPS scheme based on probabilistic amplitude shaping (PAS) architecture for improving the performance of PS signals in bandwidth-limited IMDD systems. The experimental results show that TEPS-PAM4 has up to 1.80-dB higher receiver sensitivity than PS-PAM4 at 7% forward error correction (FEC) limit with the same net rate.
- In order to reduce the computational complexity of the TEPS scheme, we further propose the constellation partition decision-assisted (CPDA)-Viterbi decoder which decides the received signal before decoding to reduce the branches. The experimental results show that with up to 45.7% reduction of multiplications compared with the Viterbi decoder, TEPS with CPDA-Viterbi decoder (TEPS-PAM4-CPDA) has up to 1.50-dB higher receiver sensitivity than PS-PAM4 at 7% FEC limit with the same net rate.

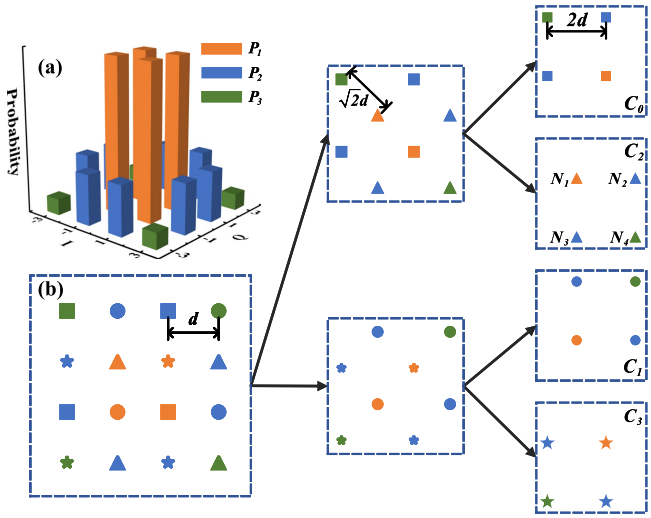

Fig. 1. Schematic diagram of subset partitioning of TEPS-PAM4. (a) Probability distribution of TEPS-PAM4 signal; (b) Two-dimensional schematic diagram of TEPS-PAM4 signal.

The rest of the article is organized as follows. In Section II, we describe in detail the structure and principles of TEPS-PAM4 and CPDA-Viterbi decoder. In Section III, the experimental setups are described and the experimental results are discussed. Then, the article is summarised in Section IV.

II. Principle

A. The Principle and Structure of TEPS-PAM4

Different from the traditional PS signal generation process, the TEPS scheme needs the subset partitioning first as shown in Fig. 1. The probability distribution of TEPS-PAM4 is shown in Fig. 1(a). In the subset partitioning, 16-point rectangular constellations are partitioned into two subsets with alternating points allocated to each subset. Assume that the minimum Euclidean distance between points is d before the set partitioning. After one subset partition, two subsets are obtained and the minimum Euclidean distance between points in each subset increases from d to $\sqrt{2}d$. By another subset partitioning, the minimum Euclidean distance between points in each subset increases further from $\sqrt{2}d$ to $2d$ and 4 subsets are obtained as C_0, C_1, C_2 and C_3.

Additionally, to be compatible with the probability impact caused by the subset partition, it is necessary to convert the probability of the transmitted signal and the signal in the subset. Taking subset C_2 as an example, there are four signal points as N_1, N_2, N_3 and N_4 and the corresponding probabilities are P_1, P_2, P_2, and P_3, as shown in Fig. 2(b). If the probabilities of each amplitude of the TEPS-PAM4 signal are P_a, P_b, P_b and P_a as

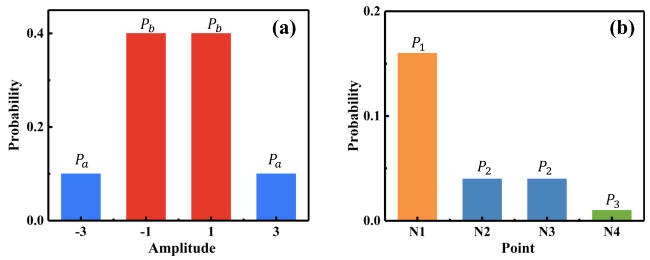

Fig. 2. Schematic diagram of the probabilities distribution of (a) PS-PAM4 and (b) four points in the subset C_2.

shown in Fig. 2(a), the P_1, P_2, P_3 and the probability of each subset can be calculated as

$$P_1 = {P_b}^2. \tag{1}$$

$$P_2 = P_a * P_b. \tag{2}$$

$$P_3 = {P_a}^2. \tag{3}$$

$$P_1 + P_2 + P_2 + P_3 = 1/4. \tag{4}$$

With (1)–(3) and $P_a + P_b = \frac{1}{2}$, (4) can be deduced which represents each subset has equal probability in the TEPS-PAM4 scheme.

The architecture of the TEPS-PAM4 scheme is shown in Fig. 3(a). The core idea is to integrate TCM into the PAS architecture to improve the bandwidth limit tolerance without affecting the distribution of PS signals. After converting the probability of the transmitted TEPS-PAM4 signal to the probability of the signal points within each subset, amplitudes with the calculated probability distribution could be generated by a constant composition distribution matching (CCDM) [38]. Then, the amplitudes with a probability distribution are transmitted to bits by a Sym2 b operation to input into the FEC encoder [21].

The λ bits which are not input into the CCDM encoding are uniform distribution and they are straightly input to the FEC encoder. After FEC encoding, the parity bits $1 - \lambda$ are combined with the λ bits as b_3 which ensures that the probabilities of b_1 and b_2 are not distorted. For a detailed introduction to PAS, please refer to ref [21]. After a convolutional encoder with the input of b_3, the redundant bit b_4 is obtained. It is worth noting that in this case b_1 and b_2 have a probability distribution, while b_3 and b_4 are uniformly distributed. Since each subset has an equal probability, b_3 and b_4 can determine the subset. The b_1 and b_2 can select the point from the chosen subset. The real part X_1 and the imaginary part X_2 of the selected two-dimensional point $X_1 + 1i \times X_2$ are transmitted as symbols of two-time slots. As a result, the mapping process of TEPS-PAM4 in this article can be summarized as shown in Table I. The different colors in the table represent different subsets.

The convolutional encoder which is a 4-state system encoder is shown in Fig. 3(b). The trellis diagram of the convolutional code is shown in Fig. 3(c), where the solid line indicates the input bit is 1 and the dashed line indicates the input bit is 0. It should be emphasized that the TEPS scheme does not lead to signal spectrum shaping. The enhanced bandwidth tolerance of this scheme relies on the embedded TCM, which improved the robustness of signal error correction.

TABLE I
MAPPING PROCESS OF TEPS-PAM4

$X_1 + 1i \times X_2$	$b_1b_2b_3b_4$	$X_1 + 1i \times X_2$	$b_1b_2b_3b_4$
$-3+1i\times3$	0000	$3-1i\times3$	0010
$1-1i$	1000	$-1+1i$	1010
$1+1i\times3$	0100	$-1-1i\times3$	0110
$-3-1i$	1100	$3+1i$	1110
$3+1i\times3$	0001	$-3-1i\times3$	0011
$-1-1i$	1001	$1+1i$	1011
$3-1i$	0101	$-3+1i$	0111
$-1+1i\times3$	1101	$1-1i\times3$	1111

The net rate of the PS-PAM signal can be expressed as

$$IR_{PS-PAM} = H - (1 - R_{fec}) * m \tag{5}$$

where the H is the entropy of the signal which can be adjusted, the R_{fec} is the code rate of the FEC encoder, and the m denotes the bits per symbol. However, for the TEPS-PAM4 signal, there is a convolutional encoder in addition to the FEC encoder. Thus, the net rate of the TEPS-PAM4 should be

$$IR_{TEPS-PAM} = H - (1 - R_{fec} * R_{con}) * m \tag{6}$$

where the R_{con} is the overall code rate of the convolutional encoder which is $3/4$ in this article.

In a bandwidth-limited system, the received signal suffers from mainly two kinds of system impairments: high-frequency fading caused by device bandwidth limitation and AWGN of the system. Fig. 4(a) and (c) show the frequency spectrum of the received signal and the system AWGN, respectively. Ideally, in order to fully compensate for channel impairments, the frequency response of the equalizer should be the inverse of the channel response. Fig. 4(e) shows the frequency response of the equalizer, which enhances the fading portion of the signal spectrum. After the equalizer, the high-frequency part of the received signal is basically not attenuated as shown in Fig. 4(b), and the distortion of the signal is compensated. However, the high-frequency part of the AWGN is also amplified, leading it to transition from white noise to colored noise as shown in Fig. 4(d). The current methods of embedding prior information into PS signals are primarily based on the AWGN channel. However, direct utilization of AWGN-based models in bandwidth-limited channels will lead to performance degradation. Although it is crucial to determine the introduction of prior information in bandwidth-limited channels, the solution remains elusive. Therefore, in this article, the incorporation of prior information in the experiment and computational complexity is abandoned.

B. The Principle of CPDA-Viterbi Decoder

The Viterbi decoder is needed in the receiver in the TEPS scheme due to combining with TCM. The process could be divided into two steps. In the first step, subset decoding is

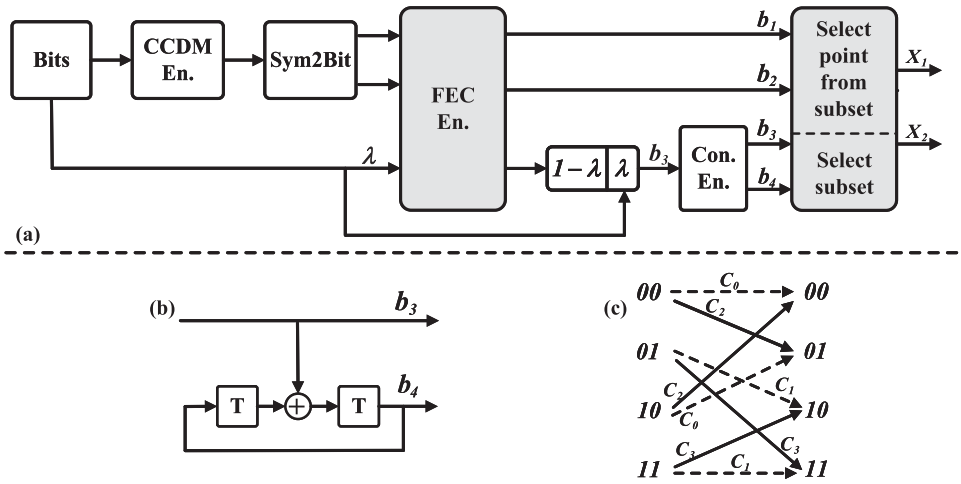

Fig. 3. Block diagram of the TEPS-PAM4 scheme. (a) The architecture of the TEPS-PAM4 scheme; (b) The architecture of the convolutional encoder; (c) The trellis diagram of the code generated by the convolutional encoder.

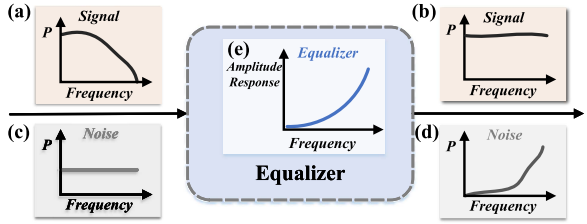

Fig. 4. Block diagram of channel equalization technology. Spectrum diagram of the signal (a) before the channel equalization and (b) after the channel equalization; Spectrum diagram of the noise (c) before the channel equalization and (d) after the channel equalization; (e) Schematic diagram of the frequency response of an adaptive filter.

performed. Each branch in the trellis corresponds to a subset, and the point in each subset that is closest to the receiving point is decided. In the second step, the squared distance metric of the point selected in the first step is used to calculate the corresponding branch of the Viterbi decoding, aiming to determine the signal path through the trellis [39].

The branch of the Viterbi algorithm of TCM can be calculated as [40]:

$$B_{C_i} = \min_{P_i^j \in C_i} |r_t - P_i^j|^2 \tag{7}$$

where the B_{C_i} is the branch whose output is subset C_i, the r_t is the received signal at time t, and the P_i^j is the jth constellation point belongs in the subset C_i. In this article, a convolutional code with a code rate of 1/2 and a memory length of 2 is adopted. 16 points are divided into 4 subsets, with each subset containing 4 points. When calculating the branch metric value of a time slot, different branch metric values may represent the same subset, and there are 4 different subsets in total. When calculating branch metrics, a received signal is calculated with up to 16 points. Moreover, when 16 points are arranged in a square formation, some repetitive calculations can be removed. As a result, the calculation of the branch metric requires 8 multiplications, 24 additions, and 12 comparisons of the minimum operation (3 for each of the 4 subsets). After calculating the branch metric, it is necessary to add the branch metric and the path metric, so 8 additions are required. The sum of the branch metric and the path metric to reach each state needs to be compared and selected once, so a total of 4 comparisons and 4 selections are required. In other scenarios, suppose the memory length of the convolutional code is L. The complexity of the branch metric remains unchanged, as the 2D-PAM4 still comprises 16 points. The convolutional encoder adopted in this article has an input length of 1. Thus, regardless of the value of L, only two branches lead to a state in the trellis diagram. But the addition calculation brought by the addition of path metrics and branch metrics will change to 2^{L+1}, and the comparison and selection will change to 2^L. Even if repeated calculations are removed, the computational complexity of the Viterbi decoder is still high.

To address the high complexity of the Viterbi decoder, we propose the CPDA-Viterbi decoder to reduce the computational burden. As shown in Fig. 5(a), the entire constellation area is divided into several small regions, which can be divided into three categories: 1) constellation points within them are directly decided as belonging to one subset, 2) constellation points within them are considered to belong to only two subsets, and 3) constellation points within them may belong to any of the subsets. The detailed schematic diagram inside the grey dotted box in Fig. 5(a) is shown in Fig. 5(b). In Fig. 5(b), the square constellation point, the round constellation point, the triangular constellation point and the star-shaped constellation point belong to subset C_0, C_1, C_2 and C_3 respectively. If the received signal at time t exists in the pink shaded region H_0, it is decided to belong to the subset C_0. In this case, only the branches of the subset C_0 need to be calculated, so the trellis diagram will change from Figs. 3(c) to 6(a). Similarly, if the received signal at time t exists in the pink shaded region H_1, H_2 and H_3, it is decided to belong to the subset C_1, C_2 and C_3, respectively. At the same time, the branches of the trellis of the corresponding subset need to be calculated as shown in Figs. 6(b)–(d). If the received signal at time t exists in the blue shaded region R_0, it may belong to any subset since the distances between each subset are similar, so the trellis is as

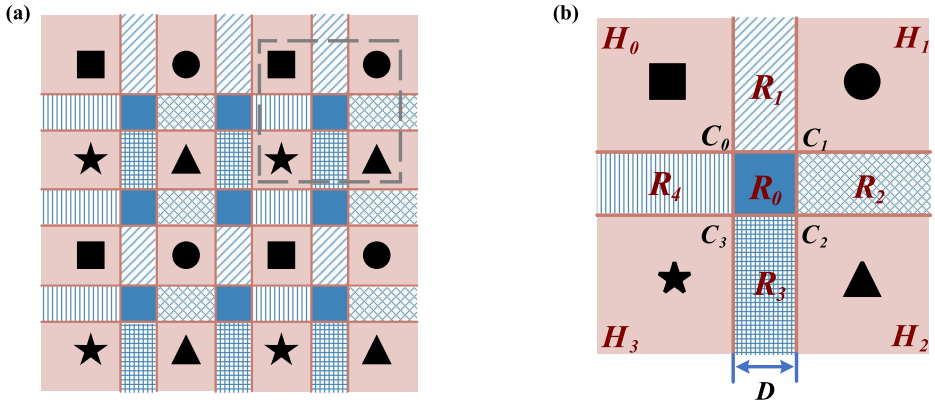

Fig. 5. Schematic diagram of the decider in CPDA-Viterbi decoder. (a) Overall diagram of the decider; (b) Details inside the grey dotted line box in (a).

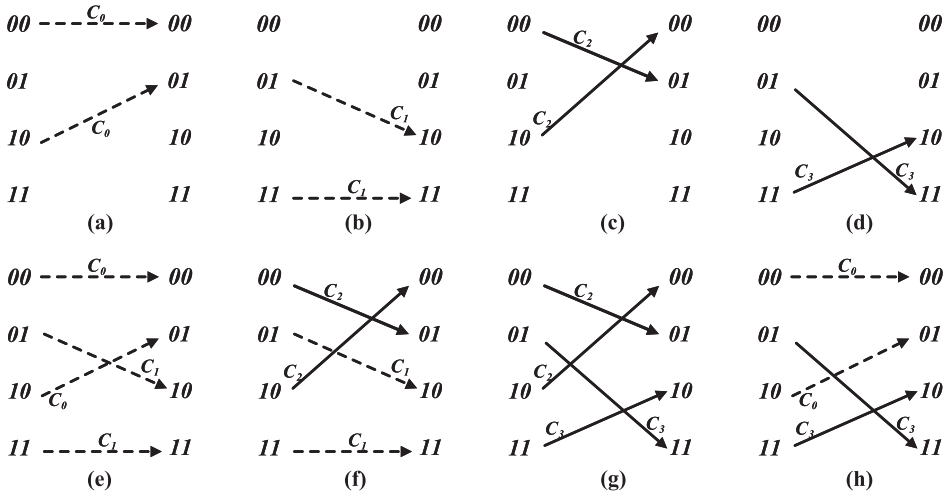

Fig. 6. Schematic diagrams of simplified trellis for the received TEPS-PAM4 signal within the area (a) H_0; (b) H_1; (c) H_2; (d) H_3; (e) R_1; (f) R_2; (g) R_3; and (h) R_4.

same as that of the Viterbi decoder. However, if the received signal exists in the blue-shaded region R_1, it is more likely to belong to the subset C_0 and C_1 because the distances to these subsets are closer than the distances to the subset C_2 and C_3. In this case, only the branches of the subset C_0 and C_1 need to be calculated, so the trellis diagram will change to Fig. 6(e). If the received signal exists in the blue-shaded region R_2, it is more likely to belong to the subset C_1 and C_2, and the trellis will turn as shown in Fig. 6(f). If the received signal exists in the blue-shaded region R_3, the trellis will become Fig. 6(g) since it is more likely to belong to the subset C_2 and C_3. Similarly, the received signal is more likely to belong to the subset C_3 and C_0 if it exists in the blue-shaded region R_3, and the trellis will turn as shown in Fig. 6(h). The thresholds are $-2 \pm \frac{D}{2}$, $0 \pm \frac{D}{2}$, and $2 \pm \frac{D}{2}$, and the D requires a trade-off between computational complexity and performance. It is worth noting that the simplification of the trellis at the receiver is only to reduce the complexity of decoding, and has no effect on the encoding at the transmitter.

After the signal is decided by the decider, the trellis for the CPDA-Viterbi decoder is simplified so that the computational complexity can be reduced. As shown in Fig. 5(b), the received signal is divided into three regions: H region, R region, and R_0 region. When the signal is in the H region, it is considered to belong to only a certain subset. Thus, when calculating the branch metric, only 4 multiplications, 8 additions, and 3 comparisons are required. After the branch metric is calculated, adding the branch metric to the path metric requires 2 additions where $L = 2$, which are 2^{L-1} additions in more general. No comparison and selection between branches is required because of the simplified trellis. When the signal is in the R region, it is considered to belong to certain two subsets. Thus, when calculating the branch metric, only 6 multiplications, 14 additions, and 6 comparisons are required. After the branch metric is calculated, adding the branch metric to the path metric requires 4 additions where $L = 2$, which are 2^L additions more generally, and no comparison and selection between branches is required. When the signal is in the R_0 region, the calculation of the complexity is the same as that of the Viterbi decoder. Additionally, for the CPDA-Viterbi decoder, the computational complexity in the decider needs to be considered. There are 12 thresholds in the decider, where 6 thresholds are used for the real part of the signal and the other 6 thresholds are used for the imaginary part of the signal. The bisection method is used to decide the signal in this

TABLE II
COMPLEXITY COMPARISON WITH VITERBI DECODER

	Viterbi Decoder	CPDA-Viterbi Decoder
Number of multiplications	8	$8-4\times Q_H-2\times Q_R$
Number of additions	$36+2^{L+2}$	$46+2^{L+2}-(25+7\times 2^{L-1})\times Q_H-(16+3\times 2^{L})\times Q_R$

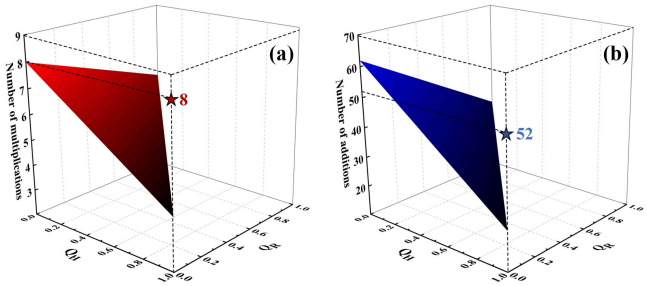

Fig. 7. Influence of different Q_H and Q_R on overall complexity when L is 2. (a) The number of the multiplications; (b) The number of the additions.

article, so the real part and the imaginary part need at most 3 comparisons and 2 selections respectively.

Suppose Q_H, Q_R, and Q_{R_0} represent the ratio of the number of signals within the region H, region R, and region R_0, respectively. These ratios are related to the distance D between the threshold values in the decider. Since the sum of Q_H, Q_R, and Q_{R_0} is 1, the Q_{R_0} can be represented by Q_H and Q_R, as shown in 8. After derivation, the complexity comparison between the CPDA-Viterbi decoder and the Viterbi decoder is shown in Table II. It is worth noting that the complexity of comparison, selection, addition and subtraction is the same [41], [42], so these operations are included in addition operations when analyzing the complexity. In this article, L is set to 2. By changing Q_H and Q_R, Table II can be visualized as shown in Fig. 7 for a clearer comparison. Specifically, Fig. 7(a) illustrates the change in the number of multiplications in which the pentagram indicates that the number of multiplications for the Viterbi decoder is 8, and Fig. 7(b) depicts the change in the number of additions in which the pentagram indicates that the number of additions for the Viterbi decoder is 52. When both Q_H and Q_R are 0, the CPDA-Viterbi decoder has the largest number of multiplications and additions, with a maximum value of 8 and 62, respectively. The maximum number of additions is greater than that of the Viterbi decoder because of the complexity of the decider. When Q_H is 1 and Q_R is 0, the CPDA-Viterbi decoder has the smallest number of multiplications and additions, with a minimum value of 4 and 13, respectively.

$$Q_{R_0}=1-Q_H-Q_R \tag{8}$$

III. EXPERIMENTAL SETUPS AND RESULTS

Fig. 8 depicts the experimental setups of a 32-GBaud IMDD system with a 10G-class O-band DML over 20-km SSMF transmission, which is used to evaluate the performance of the proposed scheme. The probability statistics of TEPS-PAM4 with the entropy of 1.9 b/symbol are shown in Fig. 8(a), and the

TABLE III
ENTROPIES AND NET RATES OF THE TRANSMITTED SIGNAL AT THE BAUD RATE OF 32 GBAUD WITH 7% OVERHEAD FEC

Net rate (bit/s)	41.6	38.4	35.2
Entropy of TEPS-PAM4 (bit/symbol)	1.9	1.8	1.7
Entropy of PS-PAM4 (bit/symbol)	1.43	1.33	1.23

horizontal axes represent the amplitude in the electrical domain or the intensity in the optical domain, respectively. In the optical domain, the light intensity cannot be negative. Fig. 9 shows the mathematical model diagram of the transmitter of the IMDD optical transmission system. The digital bipolar real signal $S(k)$ is generated by digital signal processing at the transmitter, and $S(k)$ includes positive and negative values. After digital-analog conversion (D/A), the digital bipolar real signal $S(k)$ is converted to an analog electrical signal $S(t)$. Since the information in the intensity modulation system is transmitted through the light intensity, the electrical signal to be sent needs to be a non-negative real signal, so a DC bias needs to be added before the electro-optical conversion (E/O) to ensure that the signal is a non-negative real value. Then, the non-negative real electrical signal is modulated on the optical carrier to obtain the light signal O(t) by E/O. The amplitude in Fig. 8(a) is corresponding to the digital bipolar real signal $S(k)$, and the light intensity is corresponding to the optical intensity signal $O(t)$. Fig. 8(b) shows the eye diagram of TEPS-PAM4 with the entropy of 1.9 b/symbol at the received optical power (ROP) of -11 dBm. For a fair comparison, the net rate of PS-PAM4 and TEPS-PAM4 should be equal. In this article, the overhead of FEC is 7%, and the overall code rate of the convolutional code used in the TEPS-PAM4 scheme is $3/4$. Combining (5) and (6) yields that the entropy of the TEPS-PAM4 signal should be greater by about 0.47 b/symbol than that of the PS-PAM4 signal to ensure that the net rates of the two modulation schemes are equal. For a clear illustration, the net rates and entropy values corresponding to the three cases are summarized in Table III.

The digital TEPS-PAM4 and PS-PAM4 signals are generated and pulse shaped by a root-raised cosine filter with a roll-off factor of 0.1 at the transmitter. Then, the digital signal is fed into a 64-GSa/s 8-bit digital-to-analog converter (DAC) with 3-dB bandwidth of 15-GHz to obtain an analog electrical signal. The signal is amplified by an electrical amplifier (EA) and then modulated directly by a DML with 10-GHz bandwidth at the central wavelength of 1310 nm. For the wavelength of 1310 nm, the dispersion coefficient of optical fiber is close to 0 ps/(nm·km). Therefore, the impact of dispersion on the signal can usually be ignored in the experimental system. Afterwards,

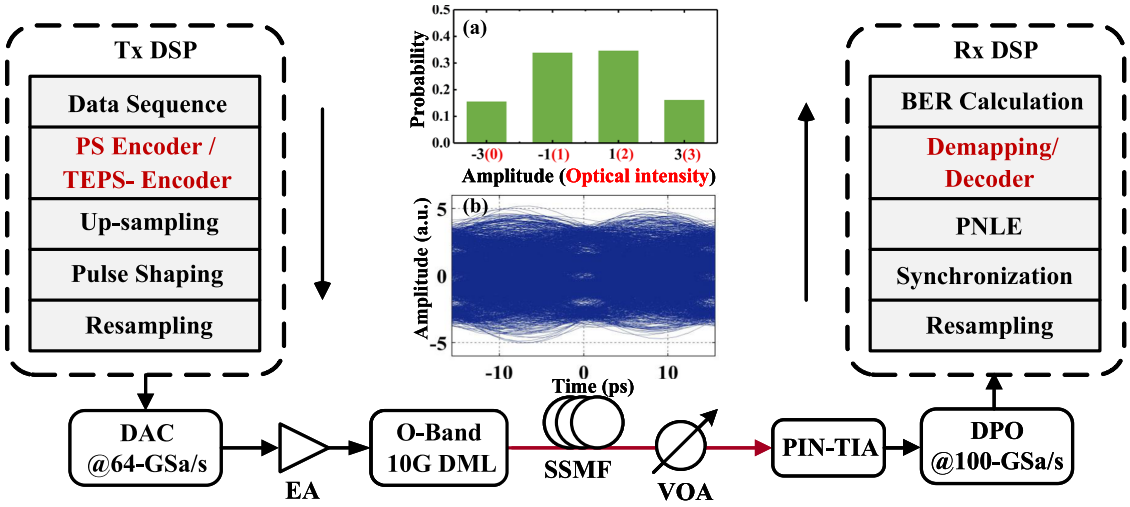

Fig. 8. Experimental setups of 32-GBaud IMDD system over 20-km SSMF with a 10G-class DML. (a) Symbol distribution of TEPS-PAM4 with the entropy of 1.9 b/symbol; (b) The eye diagram of the TEPS-PAM4 signal with the entropy of 1.9 b/symbol at the ROP of −11 dBm. DAC: Digital to analog converter; VOA: Variable optical attenuator; PIN-TIA: PIN photodiode with an integrated trans-impedance amplifier; DPO: Digital phosphor oscilloscope.

TABLE IV
BANDWIDTH OF EACH DEVICE IN THE EXPERIMENTAL SETUPS OF THE 32-GBAUD TEPS-PAM4 SYSTEM

Device	DAC	EA	DML	PIN-TIA	RTO
Bandwidth (GHz)	15 (3-dB)	25 (3-dB)	10 (3-dB)	35 (3-dB)	20 (Cut-off)

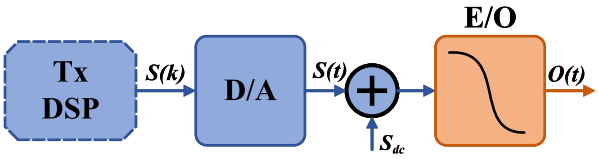

Fig. 9. Mathematical model diagram of the transmitter of the IMDD optical transmission system.

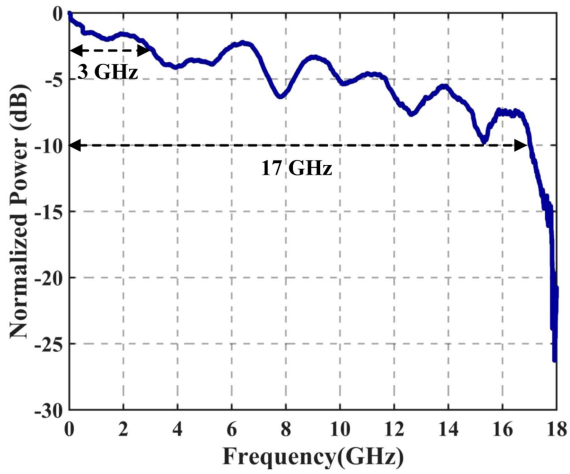

Fig. 10. Frequency response of the 32-GBaud TEPS-PAM4 system over 20-km SSMF transmission.

the optical signal is fed into the 20-km SSMF with a launch power of 9.82 dBm. A variable optical attenuator (VOA) is used to adjust the ROP at the receiver. The optical signal is transformed into an electrical signal by a PIN photodiode packaged with a trans-impedance amplifier (PIN-TIA). The obtained electrical signal is then digitized and stored by a 100-GSa/s 8-bit digital phosphor oscilloscope (DPO) with 20-GHz bandwidth. The bandwidth of each device in the experimental setups is summarized as shown in Table IV, and the frequency response of the experimental system is affected by all devices together as shown in Fig. 10. The 3-dB bandwidth of the experimental setups is about 3 GHz, and the 10-dB bandwidth is about 17 GHz. With the roll-off factor is 0.1, the bandwidth of the 32-GBaud signal is 17.8 GHz, thus the signal is subjected to strict bandwidth limitation. The receiver DSP mainly includes resampling, synchronization, channel equalization, demapper for the PS-PAM4 signal, Viterbi decoder and CPDA-Viterbi decoder for the TEPS-PAM4 signal, and bit error rate (BER) calculation. To mitigate both linear and nonlinear distortions, the polynomial nonlinear equalizer (PNLE) is adopted as channel equalization [43], and the parameters of the PNLE are (71,3,0) in this article.

Fig. 11 depicts the distance between the decision thresholds D in the TEPS-PAM4-CPDA scheme verse the performance at the ROP of −14 dBm with the entropy of 1.9 b/symbol, 1.8 b/symbol and 1.7 b/symbol. The left axis represents BER and the right axis represents the multiplication complexity reduction of the CPDA-Viterbi decoder compared with the Viterbi decoder which can expressed as $\frac{Q_H}{2} + \frac{Q_R}{4}$. The horizontal axis is the distance between the decision thresholds D, which determines

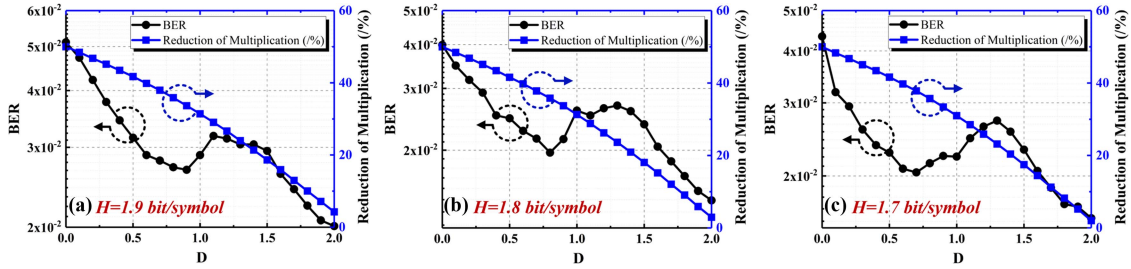

Fig. 11. BER versus D in TEPS-PAM4-CPDA scheme of 32-GBaud IMDD system over 20-km SSMF at ROP of −14 dBm with the entropy of (a) 1.9 b/symbol, (b) 1.8 b/symbol and (c) 1.7 b/symbol.

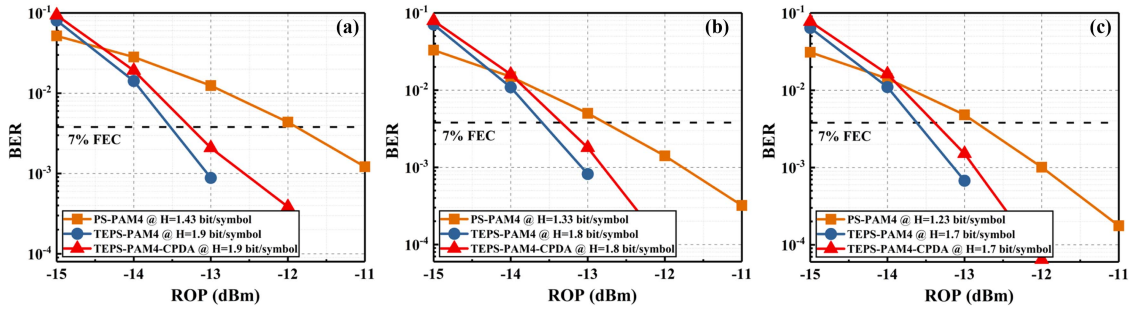

Fig. 12. BER performance comparison between the TEPS-PAM4 scheme, the TEPS-PAM4-CPDA scheme, and the PS-PAM4 scheme of 32-GBaud IMDD system over 20-km SSMF with the TEPS-PAM4 entropy of (a) 1.9 b/symbol, (b) 1.8 b/symbol and (c) 1.7 b/symbol.

how many constellation points are directly decided and thus affects the reduction in complexity and overall performance, varying from 0 to 2 in steps of 0.1. As shown in Fig. 11, as the D increases, the complexity reduction decreases, but the change of performance is non-monotonic. In order to achieve a trade-off between performance and complexity, D is set to 0.7 when the entropy is 1.7 b/symbol, and D is still set to 0.8 when the entropy is 1.8 b/symbol and 1.9 b/symbol. In theory, as the entropy decreases, the optimal value of D should decrease. However, in the experimental results, the relationship between the optimal D value and the entropy is not clearly observed due to the limited variation in entropy values and the fluctuations in experimental data, which may obscure the trend of change.

Fig. 12 reveals the BER performance comparison between the TEPS-PAM4 scheme, the TEPS-PAM4-CPDA scheme, and the PS-PAM4 scheme of 32-GBaud IMDD system over 20-km SSMF. Under the same net rate conditions, the entropies of the TEPS-PAM4 signal are 1.9 b/symbol, 1.8 b/symbol, and 1.7 b/symbol, while the corresponding entropies of the PS-PAM4 signal are 1.43 b/symbol, 1.33 b/symbol, and 1.23 b/symbol, respectively. When the entropy of the TEPS-PAM4 signal is 1.9 b/symbol and the entropy of the PS-PAM4 signal is 1.43 b/symbol, the ROP verse BER is shown in Fig. 12(a). The ROP of the TEPS-PAM4 scheme and the PS-PAM4 scheme is −13.60 dBm and −11.80 dBm at the 7% FEC limit, respectively. Therefore, compared with PS-PAM4, the TEPS-PAM4 scheme achieves about 1.80-dB higher receiver sensitivity. With the low-complexity CPDA-Viterbi decoder, the ROP of the TEPS-PAM4-CPDA is −13.30 dBm at the 7% FEC limit. Thus, the TEPS-PAM4-CPDA achieves about 1.50-dB higher receiver sensitivity than the PS-PAM4 scheme. As the penalty of the reduced complexity, there is a 0.30-dB ROP penalty of the TEPS-PAM4-CPDA compared with the TEPS-PAM4 scheme which used the traditional Viterbi decoder. The ROP verse BER with the TEPS-PAM4 signal entropy of 1.8 b/symbol and the PS-PAM4 signal entropy of 1.33 b/symbol is shown in Fig. 12(b). Under these conditions, the TEPS-PAM4 scheme has 0.90-dB higher receiver sensitivity than PS-PAM4, and the TEPS-PAM4-CPDA scheme achieves about 0.60-dB higher receiver sensitivity than PS-PAM4, since the ROP of the TEPS-PAM4 scheme, the TEPS-PAM4-CPDA scheme, and the PS-PAM4 scheme is −13.65 dBm, −13.35 dBm and −12.75 dBm at the 7% FEC limit, respectively. The ROP verse BER with the TEPS-PAM4 signal entropy of 1.7 b/symbol and the PS-PAM4 signal entropy of 1.23 b/symbol is shown in Fig. 12(c). At the 7% FEC limit, the ROPs of the TEPS-PAM4 scheme, the TEPS-PAM4-CPDA scheme, and the PS-PAM4 scheme are −13.70 dBm, −13.40 dBm and −12.80 dBm, respectively. Therefore, compared with the PS-PAM4 scheme, the TEPS-PAM4 scheme achieves about 0.90-dB higher receiver sensitivity and the TEPS-PAM4-CPDA scheme achieves about 0.60-dB higher receiver sensitivity at the 7% FEC limit.

Fig. 13(a) and (b) respectively show the multiplication and addition reduction of the CPDA-Viterbi decoder compared to the Viterbi decoder with the entropy of TEPS-PAM4 signal of 1.9 b/symbol, 1.8 b/symbol, and 1.7 b/symbol. The complexity reduction increases with the ROP, regardless of the entropy of the TEPS-PAM4 signal. When the ROP is low, i.e. −15 dBm, the constellation points of the received signal are blurred, making it difficult to determine which subset the received signal belongs

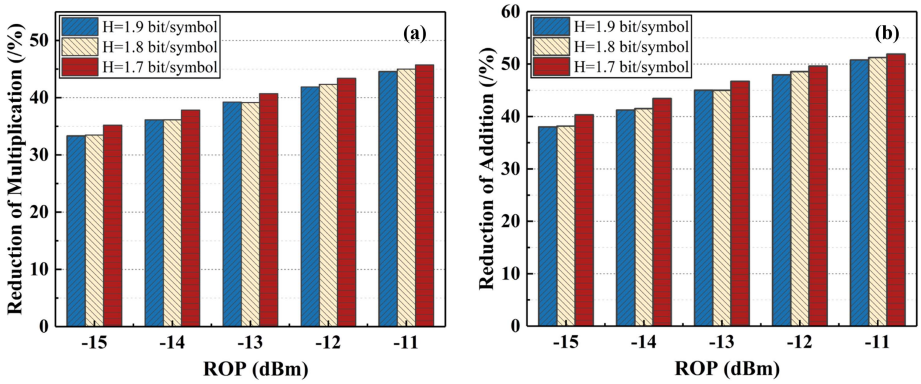

Fig. 13. Complexity reduction of CPDA-Viterbi decoder compared to Viterbi decoder versus ROP with the TEPS-PAM4 entropy of 1.9 b/symbol, 1.8 b/symbol and 1.7 b/symbol. (a) Reduction of multiplication; (b) Reduction of addition.

to. When the ROP is high, i.e. −11 dBm, the constellation points of the received signal become clearer and easier to determine which subset it belongs to. When the entropy of the TEPS-PAM4 signal is 1.9 b/symbol, the maximum multiplication reduction and addition reduction are 44.6% and 50.8%, respectively. When the TEPS-PAM4 signal entropy is 1.8 b/symbol, the maximum multiplication reduction and addition reduction are 45.0% and 51.2%, respectively. With the TEPS-PAM4 signal entropy of 1.7 b/symbol, the maximum multiplication reduction and addition reduction are 45.7% and 51.9%, respectively. Therefore, the experimental results prove that adopting CPDA-Viterbi decoding instead of the Viterbi decoder algorithm can greatly reduce computational complexity.

IV. Conclusion

In this article, the TEPS scheme with CPDA-Viterbi decoder is proposed for improving the performance of the PS signals with low complexity in bandwidth-limited IMDD systems. The performance of the proposed scheme is verified on a 32-GBaud IMDD optical transmission system over 20-km SSMF with a 10G-class O-band DML. The experimental results show that, when the entropies of TEPS-PAM4 are 1.9 b/symbol, 1.8 b/symbol, and 1.7 b/symbol, compared with the PS-PAM4 scheme, at the 7% FEC limit, the receiver sensitivity gains of TEPS-PAM4 scheme are 1.80 dB, 0.90 dB, and 0.90 dB, respectively. Moreover, by applying the proposed CPDA-Viterbi decoder instead of the Viterbi decoder, the multiplication complexity and addition complexity can be reduced by up to 45.7% and 51.9%, respectively. Compared with the PS-PAM4 scheme, when the entropies of TEPS-PAM4 are 1.9 b/symbol, 1.8 b/symbol, and 1.7 b/symbol, the TEPS-PAM4-CPDA scheme could achieve about 1.50-dB, 0.60-dB, and 0.60-dB higher receiver sensitivity, respectively. Therefore, the proposed TEPS-PAM4-CPDA scheme shows great potential to realize high-performance, low-cost bandwidth-limited IMDD systems.

References

[1] Y. Yu, Y. Che, T. Bo, D. Kim, and H. Kim, "Reduced-state MLSE for an IM/DD system using PAM modulation," *Opt. Exp.*, vol. 28, no. 26, pp. 38505–38515, 2020.

[2] M. Chen, L. Wang, D. Xi, L. Zhang, H. Zhou, and Q. Chen, "Comparison of different precoding techniques for unbalanced impairments compensation in short-reach DMT transmission systems," *J. Lightw. Technol.*, vol. 38, no. 22, pp. 6202–6213, Nov. 2020.

[3] L. Zhang et al., "Real-time demonstration of a low-complexity PS scheme for 16QAM-DMT signals in an IM-DD system," *Opt. Exp.*, vol. 31, no. 7, pp. 11447–11456, 2023.

[4] J. Cheng, C. Xie, Y. Chen, X. Chen, M. Tang, and S. Fu, "Comparison of coherent and IMDD transceivers for intra datacenter optical interconnects," in *Proc. IEEE Opt. Fiber Commun. Conf. Exhib.*, 2019, pp. 1–3.

[5] C. Bluemm, M. Schaedler, M. Kuschnerov, F. Pittalà, and C. Xie, "Single carrier vs. OFDM for coherent 600 Gb/s data centre interconnects with nonlinear equalization," in *Proc. IEEE Opt. Fiber Commun. Conf.*, 2019, pp. 1–3.

[6] W. Shieh, C. Sun, and H. Ji, "Carrier-assisted differential detection," *Light: Sci. Appl.*, vol. 9, no. 1, 2020, Art. no. 18.

[7] K. Wang, M. Zhao, M. Kong, and J. Yu, "Demonstration of 4× 100 Gbit/s PAM-4 transmission over 40 km in an IM/DD system based on narrow band DMLs," *IEEE Photon. J.*, vol. 12, no. 3, Jun. 2020, Art no. 7201908.

[8] C. Huang et al., "Optical multipath interference mitigation for high-speed PAM4 IMDD transmission system," *J. Lightw. Technol.*, vol. 40, no. 16, pp. 5490–5501, Aug. 2022.

[9] J. Yu et al., "Applications of 40-Gb/s chirp-managed laser in access and metro networks," *J. Lightw. Technol.*, vol. 27, no. 3, pp. 253–265, Feb. 2009.

[10] N. T. Hung et al., "High-speed PAM4 transmission using directly modulated laser and artificial neural network nonlinear equaliser," *Opt. Laser Technol.*, vol. 157, 2023, Art. no. 108642.

[11] E. Giacoumidis, A. Kavatzikidis, A. Tsokanos, J. Tang, and I. Tomkos, "Adaptive loading algorithms for IMDD optical OFDM PON systems using directly modulated lasers," *J. Opt. Commun. Netw.*, vol. 4, no. 10, pp. 769–778, 2012.

[12] J. Wei et al., "Experimental comparison of modulation formats for 200 G/λ IMDD data centre networks," in *Proc. IEEE 45th Eur. Conf. Opt. Commun.*, 2019, pp. 1–4.

[13] T. Gui et al., "Real-time single-carrier 800 Gb/s DP-64QAM demonstration using bi-directional self-homodyne coherent transceivers with 200krad/s endless active polarization controller," in *Proc. IEEE Optoelectron. Commun. Conf.*, 2021, pp. 1–3.

[14] J. Renaudier et al., "Multi rate IMDD transceivers for optical interconnects using coded modulation," in *Proc. IEEE Opt. Fiber Commun. Conf. Exhib.*, 2016, pp. 1–3.

[15] Y. Fu et al., "Computationally efficient 120 Gb/s/λ PWL equalized 2D-TCM-PAM8 in dispersion unmanaged DML-DD system," in *Proc. IEEE Opt. Fiber Commun. Conf. Exhib.*, 2020, pp. 1–3.

[16] M. Chagnon, M. Morsy-Osman, M. Poulin, C. Paquet, S. Lessard, and D. V. Plant, "Experimental parametric study of a silicon photonic modulator enabled 112-Gb/s PAM transmission system with a DAC and ADC," *J. Lightw. Technol.*, vol. 33, no. 7, pp. 1380–1387, Apr. 2015.

[17] S. Yamamoto, H. Taniguchi, A. Matsushita, M. Nakamura, S. Okamoto, and Y. Kisaka, "Spectral-shaping technique based on nonlinear-coded-modulation for short-reach optical transmission," *J. Lightw. Technol.*, vol. 38, no. 2, pp. 466–474, Jan. 2020.

[18] S. Yamamoto, H. Taniguchi, M. Nakamura, and Y. Kisaka, "Nonlinear differential coding for spectral shaping of PAM signal in high-baudrate short-reach optical transmission," *J. Lightw. Technol.*, vol. 39, no. 4, pp. 1064–1071, Feb. 2021.

[19] D. A. A. Mello, F. A. Barbosa, and J. D. Reis, "Interplay of probabilistic shaping and the blind phase search algorithm," *J. Lightw. Technol.*, vol. 36, no. 22, pp. 5096–5105, Nov. 2018.

[20] D. Semrau et al., "Achievable information rates estimates in optically amplified transmission systems using nonlinearity compensation and probabilistic shaping," *Opt. Lett.*, vol. 42, no. 1, pp. 121–124, 2017.

[21] G. Böcherer, F. Steiner, and P. Schulte, "Bandwidth efficient and rate-matched low-density parity-check coded modulation," *IEEE Trans. Commun.*, vol. 63, no. 12, pp. 4651–4665, Dec. 2015.

[22] J. Zhou et al., "First 100 Gb/s fine-granularity flexible-rate PON based on discrete multi-tone and PAPR optimization," in *Proc. IEEE Opt. Fiber Commun. Conf.*, 2022, pp. 1–3.

[23] R. Borkowski et al., "Operator trial of 100 gbit/s FLCS-PON prototype with probabilistic shaping and soft-input FEC," in *Proc. IEEE Eur. Conf. Opt. Commun.*, 2021, pp. 1–4.

[24] T. Liu, J. Ma, J. Lu, J. Liu, X. Zeng, and Y. Wang, "Performance enhanced probabilistically shaped PAM4 signal based on nonlinear differential coding for IM/DD system," *Opt. Fiber Technol.*, vol. 71, 2022, Art. no. 102907.

[25] D. Che, J. Cho, and X. Chen, "Does probabilistic constellation shaping benefit IM-DD systems without optical amplifiers?," *J. Lightw. Technol.*, vol. 39, no. 15, pp. 4997–5007, Aug. 2021.

[26] M. S.-B. Hossain et al., "Probabilistic Shaping for High-Speed Unamplified IM/DD Systems with an O-Band EML," *J. Lightw. Technol.*, vol. 41, no. 16, pp. 5373–5382, Aug. 2023.

[27] B. Di, L. Song, and Y. Li, "Trellis coded modulation for non-orthogonal multiple access systems: Design, challenges, and opportunities," *IEEE Wireless Commun.*, vol. 25, no. 2, pp. 68–74, Apr. 2018.

[28] Y. Bai et al., "Performance-enhanced three-dimensional trellis coded modulation based on four-winged fractional-order chaotic encryption for physical layer security," *J. Lightw. Technol.*, vol. 40, no. 24, pp. 7701–7710, Dec. 2022.

[29] X. Qin et al., "Recurrent neural network based joint equalization and decoding method for trellis coded modulated optical communication system," *J. Lightw. Technol.*, vol. 41, no. 6, pp. 1734–1741, Mar. 2023.

[30] G. Ungerboeck, "Trellis-coded modulation with redundant signal sets Part I: Introduction," *IEEE Commun. Mag.*, vol. 25, no. 2, pp. 5–11, Feb. 1987.

[31] Y. Fu et al., "25 Gbps two-dimensional trellis coded PAM4 TDM-PON transmission based on 10 G optics," in *Proc. IEEE Opto- Electron. Commun. Conf. Photon. Glob. Conf.*, 2017, pp. 1–2.

[32] H. Cui, S. Liu, Y. Lu, and Y. Qiao, "Experimental demonstration of 2D-Trellis coded modulation PAM8 for 50 G PON based on 10G-class O-band DML," in *Proc. IEEE 27th OptoElectronics Commun. Conf. Int. Conf. Photon. Switching*, 2022, pp. 1–3.

[33] N. Stojanović et al., "4D PAM-7 trellis coded modulation for data centers," *IEEE Photon. Technol. Lett.*, vol. 31, no. 5, pp. 369–372, Mar. 2019.

[34] M. Xiang et al., "Experimental study of performance enhanced IM/DD transmissions combining 4D trellis coded modulation with precoding," *Opt. Exp.*, vol. 26, no. 25, pp. 32522–32531, 2018.

[35] S. Alreesh, C. Schmidt-Langhorst, R. Emmerich, P. W. Berenguer, C. Schubert, and J. K. Fischer, "Four-dimensional trellis coded modulation for flexible optical communications," *J. Lightw. Technol.*, vol. 35, no. 2, pp. 152–158, Jan. 2017.

[36] *A Modem Operating at Data Signalling Rates of up to 33 600 Bit/s for Use on the General Switched Telephone Network and on Leased Point-to-Point 2-Wire Telephone-Type Circuits*, ITU-T Recommendation V.34, 1998.

[37] *Multi-Gigabit Fast Access to Subscriber Terminals (MGfast)–Physical Layer Specification*, ITU-T Recommendation G.9711 Amendment 1, 2022.

[38] P. Schulte and G. Böcherer, "Constant composition distribution matching," *IEEE Trans. Inf. Theory*, vol. 62, no. 1, pp. 430–434, Jan. 2016.

[39] J. G. Proakis and M. Salehi, *Digital Communications*, vol. 4. New York, NY, USA: McGraw-hill, 2001.

[40] S. M. Alamouti, V. Tarokh, and P. Poon, "Trellis-coded modulation and transmit diversity: Design criteria and performance evaluation," in *Proc. IEEE Int. Conf. Universal Pers. Commun. Conf. Proc.*, 1998, pp. 703–707.

[41] S. Jain, X. Jia, A. F. Sabili, and F. Stephan, "Addition machines, automatic functions and open problems of Floyd and Knuth," *J. Comput. Syst. Sci.*, vol. 136, pp. 135–156, 2023.

[42] T. H. Cormen, C. E. Leiserson, R. L. Rivest, and C. Stein, *Introduction to Algorithms*. Cambridge, MA, USA: MIT Press, 2022.

[43] X. Tang et al., "An efficient nonlinear equalizer for 40-Gb/s pam4-pon systems," in *Proc. IEEE Opt. Fiber Commun. Conf. Expo.*, 2018, pp. 1–3.